The Effect of Angle of Attack and Chord Length of the Foil on Winged Air Induction Pipe Optimization toward Drag Reduction by using Numerical Approach

Yanuar[1*], Muhammad Alief[1], M. Akbar[1], Fatimatuzzahra[1], and Made[1]
[1]*Department of Mechanical Engineering, University of Indonesia, Depok, Indonesia*

Keywords: Micro-bubble, Winged Air Induction Pipe (WAIP), foil, Angle of Attack, Chord Length, Drag Reduction.

Abstract: In response to achieve better energy efficiency on the ship we propose the usage of air lubrication to reduce ship drag. Winged Air Induction Pipe (WAIP) device that we used, will create micro-bubble to coat the bottom of the ship by pulling air through induction pipe. Because of this phenomenon the drag reduction will occur. The customization placement of the foil will give the different result of drag reduction experienced by plate located after the foil. But, on this research we will see the different results of drag reduction caused by angle of attack of the foil and its chord length. By using k-ω SST (shear stress transport) model on ANSYS 2-D fluent in our numerical simulation we can see how those customization and setup affect the result. On the analysis we see the correlation between chord length and angle of attack of the foil that give most efficiency for the ship. With this setup the drag reduction reach 3% of efficiency.

1 INTRODUCTION

Ships are the most important aspect on the distribution of goods all around the world. According to Hydros Foundation, there are 50.000 Cargo ships that sail every day. All of those ships burn around 150 to 300 tons of fuel each day and produce 120 million tons of carbon dioxide emission gas every year. Even though it creates such an efficient way on transferring goods, it becomes such the biggest contributor on why global warming happens.

Many efforts have been taken to reduce the consumption of fuel and emission gases. One of which is by reducing the resistances of ship so that the energy needed by ships will be much lesser. Huge impact given by friction resistance makes it one of main components needed to be reduced. Reducing friction resistance can obtain bigger velocity, save more energy over the pump system, increase efficiency, reduce fuel consumption and minimize the operational bill as well as the emission gases (Pang et al., 2014).

Speaking of which, there are 2 components that affect ship's friction resistance which also reduce the velocity of the ships, they are water density and wetted surface area of the hull. Reducing local water density can be attained by layering up the ship's hull with micro-bubble so that can lower the mean density of two phases flow in the boundary layer when the flow is turbulent (Uhlman, 1987; Yanuar et al., 2012; Zhang et al., 2018). Therefore, the reduction of local water density makes not only its viscosity much lower, but also make the Reynold shear stress.

This method of air lubrication is proved that it is able to reduce the ship's friction resistance up to 10-15% (Kodama et al., 2000). However, this reduction is accompanied by the undeniable energy needed to inject micro-bubble into the water. This energy required adiabatic compression energy, the energy to generate micro-bubble and mechanical losses in the compressor (Kumagai et al., 2015). Hence, it causes the net total reduction around 0-5% and hampers the application of the full scale ship.

To overcome this, Kumagai et al. (2015) used bubble generating device called Winged Air Induction Pipe (WAIP). Hydrofoil was attached below microbubble injector to create low pressure area on the upper surface of the hydrofoil when the ship was travelling. The low pressure could make the atmospheric air enter the flow without using compressor. Yet, there are some variables required, they are shapes and dimension of the hydrofoil, angle of attack, clearance between WAIP to the hull, flow types, etc. These relate to the relationship among variables which is difficult to imagine, so that the determination of how high

Yanuar, ., Alief, M., Akbar, M., , F. and , M.
The Effect of Angle of Attack and Chord Length of the Foil on Winged Air Induction Pipe Optimization toward Drag Reduction by using Numerical Approach.
DOI: 10.5220/0008543401190125
In *Proceedings of the 3rd International Conference on Marine Technology (SENTA 2018)*, pages 119-125
ISBN: 978-989-758-436-7

or low the variables to make the most possible optimum rate is still hard to be defined. Besides, for those bigger ships which have deep full water, pressure created is not so low, so additional blower is needed to maximize micro-bubble injection.

On their research, Kumagai et al. (2011) used angle of attack variations by the magnitude about 12°,16°,and 20°with the same length hydrofoil and injection hole. However, length required for the hydrofoil was not elaborated briefly. Therefore, this research is going to make variation on the same amount of angle of attack about 12°,16°,and 20°but with length variation of hydrofoil around 30,35,40,45,50 [mm], so that can generate different data variation each angle of attack in every length of hydrofoil. Consequently, it can be taken from optimal angle of attack and length of hydrofoil to reduce the resistances of the ship.

2 THEORY

2.1 Experimental Theory

The moving foil in a flow will result in the negative pressure of the area in the foil surface (Ockfen and Matveev, 2009). Then, atmospheric air will be pulled when the negative pressure value made higher than the hydrostatic pressure (Series A, 1779), where

$$\Delta P \geq \rho g h \tag{1}$$

where

$$\Delta P = 1/2 C_p \rho U^2 \tag{2}$$

and

$$\rho g H = (\rho - \rho_{air}) g H \tag{3}$$

In sequencing, C_p is the negative pressure coefficient in the foil, ρ is the density of fluid, U is velocity of the fluid and H is the distance from draft to the WAIP installed area.

However, the higher the value of ΔP does not determine that the bubble will be formed. So that we should still watch the limit of how fluid stream by

$$U \geq U_E \tag{4}$$

where

$$U_E \cong \sqrt{\frac{2gH}{C_p}} \tag{5}$$

Therefore, from the formula above, we can notice that it is the value of C_p which determines whether in certain condition the bubble will be formed or not. In addition, the higher the C_p value, the higher the value of P will be while the U_E will be smaller. In other words, the first requirement of drag reduction creation will be fulfilled (Cui et al., 2003)(Shereena et al., 2013). This is due to the effect of how high the value of U compare with the value of U_E when the bubble is created, which has been proved by Kumagai et al. (2015).

From the WAIP experiment in towing tank Kumagai et al. (2010) the injected energy will be smaller when meeting this formula:

$$C_p \alpha > \frac{A}{B} C_D \cong \frac{L}{h_b} C_D sin\theta \tag{6}$$

when L, h_b and θ in sequence are cord length, air bubble mixed layer, thickness, and angle of attack of hydrofoil. With this formulation, L and θ in foil adequately affect the amount of C_p value. Net power saving will be greater if the value of C_p/C_D is also greater (Kumagai et al., 2015). Therefore, by arranging L and θ foil, we will manage to get the same value of C_D as we expected then it will result in the highest net power saving in this phenomenon.

Besides, to understand whether a WAIP is able to create bubble or not, we can look at how the energies working in the installed tool area. If the W_total gets zero, it can be concluded that there is bubble without extra injection.

$$W_{total} = W_0 - W_L + W_D \tag{7}$$

W_0 is the variable which describes the energy needed to inject bubble into the stream when the energy determined by how deep the installed tool are (H) and the flux volume (Q)

$$W_0 = \rho g H Q \tag{8}$$

W_L is the variable representing the negative energy obtained by the the installment of WAIP (foil). The value of W_L is determined by how great the C_p value and certain flow velocity (U).

$$W_L = 1/2 C_p \rho U_0^2 Q \tag{9}$$

W_D represents the energy formed when the Drag force in WAIP (foil) installed. C_D in the foil and the area of the foil contacted with fluid determine the value of W_D.

$$W_D = 1/2 C_D \rho U_0^2 A \tag{10}$$

Hence, the energy forming the bubble will touch the zero point if the value of C_P in the foil is as high as possible and the value of C_D is as low as possible.

2.2 Computational Theory

Along with set-up when has been prepared, there are some formulations which can explain how this set-up is able to represent the model being made. By using RANS Reynold Averages Navier Stokes Equation we can simulate how the flow visualised in our simulation. RANS is an equation that explain how the flow and its component happen. It also describes many phenomenons such as transient, viscous, incompressible, two phase flow and three dimensional (Muste et al., 2009). The formulation is described as follow :

$$\nabla U = 0 \tag{11}$$

$$\frac{\delta \rho U}{\delta t} + \nabla(\rho U U^T) = -\nabla p* + \nabla(\mu \nabla U) + \nabla(\rho\tau) + S \tag{12}$$

where $U = (u_x + u_y + u_z)$ is the velocity vector. t is time. ∇ is vector differential factor. p^* is relative pressure. ρ and μ are fluid properties the density and the dynamic viscosity, respectively. τ is Reynold stress tensor for turbulence flow, which we will be using the k-ω SST equation for this research. With many factors and considerations we use the k-ω SST to be our main method and equation on this research.

2.2.1 SST k-ω

Generally, Shear-Stress Transport (SST) k-ω is employed as the modelling. In the consideration that this modelling can calculate more accurately on the turbulent flow near the wall, then this also correct in the advanced way relating to the roughness effect in the skin friction and thermal flux which occur on the modelling process (Olazabal-Loumé et al., 2017). Roughness is being essential since it is the roughness which causes the friction resistance, the alteration of flow formation and the velocity difference in the boundary layer. These points should be considered and emended, reckoning that the foil passing the flow will bear the phenomena above. Furthermore, this model can simulate directly two turbulence towards the wall boundary instead of correlating near wall and far field region by empirical wall function (Mohanarangam et al., 2009). The formulation is described as follow; Kinematic Eddy Viscosity

$$\nu_T = \frac{a_1 k}{max(a_1 \omega S F_2} \tag{13}$$

Turbulence Kinetic Energy

$$\frac{\delta k}{\delta t} + U \frac{\delta k}{\delta x_j} = P_k - \beta k\omega + \frac{\delta}{\delta x_j}\left[(\nu + \sigma_k \nu_T)\frac{\delta k}{\delta x_j}\right] \tag{14}$$

Specific Dissipation Rate

$$\frac{\delta \omega}{\delta t} + U_j \frac{\delta \omega}{\delta x_j} = aS^2 - \beta\omega^2 + \frac{\delta}{\delta x_j}\left[(\nu + \sigma_k \nu_T)\frac{\delta k}{\delta x_j}\right] + 2(1 - F_1)\sigma_{\omega 2}\frac{1}{\omega}\frac{\delta k}{\delta x_i}\frac{\delta \omega}{\delta x_i} \tag{15}$$

The turbulence kinetic energy k and specific dissipation rate w are estimated from the boundary condition of turbulence quantities turbulence intensity I and length scale l, where the formulation is ;

$$k = \frac{3}{2}(U_{avg} I)^2 \tag{16}$$

and

$$\omega = \frac{k^{1/2}}{c_\mu^{1/4} i} \tag{17}$$

Due to the differences in flow phases after air sucked in to the water and its mass velocity, the comparison of volume of fluid and how the bubble entering the water, this mixed flow needs to be watched on how momentum happening in every phases. Besides, to get the flow following its compressibility, mixing reactions, and mixture fraction as well as in the turbulence flow, we need to record it so that those can be explained using the formulations below;

Continuity equation of diffusion

$$\frac{\delta}{\delta t}(\rho_m) + \nabla(\rho_m \overrightarrow{v}_m) = 0 \tag{18}$$

where $\overrightarrow{v}_m$ is the mass velocity as follow;

$$\overrightarrow{v_m} = \frac{\sum_{k=1}^{n} a_k \rho_k \overrightarrow{v_k}}{\rho_m} \tag{19}$$

where ρ_m is the diffusion of density described as follow:

$$\rho_m = \sum_{k=1}^{n} a_k \rho_k \tag{20}$$

where a_k is volume fraction of the phase k.

Therefore the density distinction of the bubble formation of foil will be answered. Consequently, the density counted is not homogeneous in every situation. It also says that the density counted is not homogeneous in every situation.

Due to its curvature the upper surface foil will own distinctive velocity. Then, its flow will pull the atmospheric air in. This flow, both mixed and not, will have heterogeneous density where the flowed mass will be different. Furthermore, velocity will also be different, especially on upper and below surface foil. Therefore momentum will be created in the flow. The following is the formulation used in the modelling of SST k-ω this time.

$$\begin{aligned}&\frac{\delta}{\delta t}\left(\rho_m \vec{\nu}_m\right)+\nabla\left(\rho_m \vec{\nu}_m \vec{\nu_m}\right)\\&=-\nabla p+\nabla\left[\mu_m\left(\nabla \vec{\nu}_m+\nabla \vec{\nu}_m^T\right)\right]\\&+\rho mg+\vec{F}+\nabla\left(\sum_{k=1}^{n} a_k \rho_k \vec{\nu}_{dr,k} \vec{\nu}_{dr,k}\right)\end{aligned} \tag{21}$$

where, n is number of phases, $\vec{F}$ is body force and μ_m is the viscosity of the diffusion. Since the mixed viscosity is not homogeneous, therefore;

$$\mu_m=\sum_{k=1}^{n} a_k \mu_k \tag{22}$$

$\vec{\nu}_{dr,k}$ is drift velocity for secondary phase k, where;

$$\vec{\nu}_{dr,k}=\vec{\nu}_k-\vec{\nu}_m \tag{23}$$

where ν_k defined the dynamic viscosity of the k phase. The relative velocity is defined as the velocity of a secondary phase p relative to the velocity of the primary phase q.

$$\vec{\nu}_{pq}=\vec{\nu}_p-\vec{\nu}_q \tag{24}$$

The mass fraction of any phase k given as :

$$C_k=\frac{a_k \rho_k}{\rho_m} \tag{25}$$

Drift velocity and relative velocity $\vec{\nu}_{pq}$ connected by:

$$\vec{\nu}_{dr,p}=\vec{\nu}_{pq}-\sum_{k=1}^{n} c_k \vec{\nu}_{qk} \tag{26}$$

From the previous continuity equation for secondary phase p, the volume fraction of the secondary phase p can be obtained as :

$$\begin{aligned}&\frac{\delta}{\delta t}(\alpha_p \rho_p)+\nabla\left(\alpha_p \rho_p \nu_m\right)=-\nabla(\alpha_p \rho_p \nu_{dr,p})\\&+\sum_{k=1}^{n}\left(\dot{m}_{qp}-\dot{m}_{pq}\right)\end{aligned} \tag{27}$$

where $\dot{m}_{qp}$ and $\dot{m}_{pq}$ is the mass flow rates. Drift velocity is important to be inserted due to the flow which contacts with the plate will have different velocity.

3 COMPUTATIONAL DOMAIN

The model used is a plate with a dimension of 5000 mm in length with a thickness of 200 mm with a modification of the manufacture of 80 mm wide holes and the addition of hydrofoil at a coordinates of 2.216 mm from the bow section (Kumagai et al., 2010). The

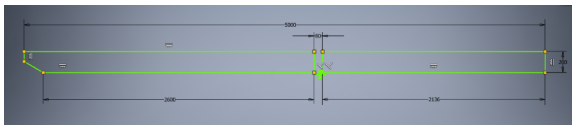

Figure 1: Model and WAIP Attachment View from z+

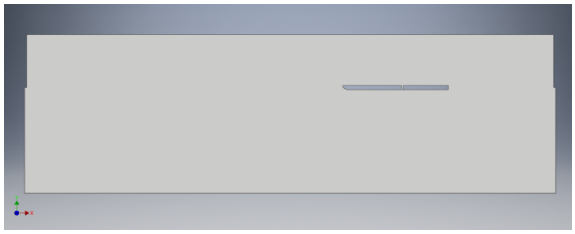

Figure 2: WAIP Design

Modeling is using the Autodesk Inventor 2018 software. Details of the model created can be seen in the picture.

The WAIP device that we used is the NACA 653 - 618 profile according to the power reduction experiment using hydrofoil (Kumagai et al., 2015). Boundary condition in this simulation has a dimension where the inlet part is placed 1-2 Lpp in front of the hull direction, the outlet part is 3-5 Lpp from the stern, and the exterior is 1 Lpp from the keel and upper exterior is 0.5 Lpp from keel (ITTC, 2011). More grid numbers does not always produced better numerical results (Gebreslassie et al., 2012). Therefore, a Grid Independency Analysis (GIA) method is used to find out the right meshing method. Determination of the right mesh size using the Grid Independency Analysis (GIA) method by comparing the results with the experimental results (Kumagai et al., 2015) with a similar model as a form of initial validation.

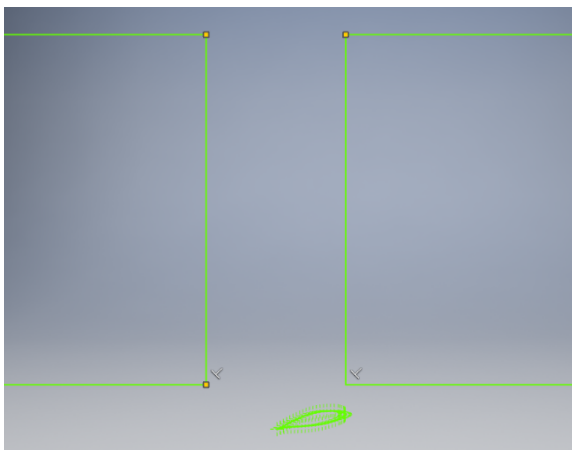

Figure 3: Boundary Condition

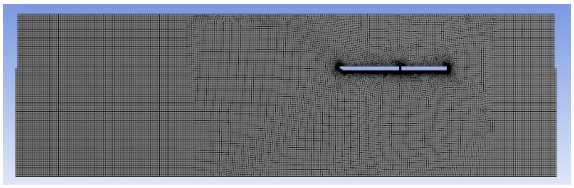

Figure 4: Meshing Model

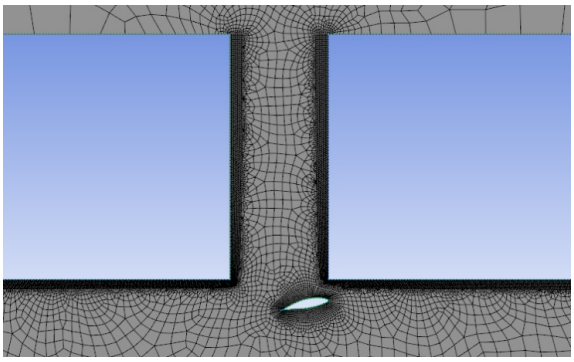

Figure 5: Zoom In of Meshing Model

4 SETUP (GRID AND DISCRETIZATION) AND VALIDATION

4.1 Setup (Grid and Discretization)

At the first time, we have to choose which resolution of grid we want to use. Because, good results depends on good quality of meshing. To determine the quality of the grid, we can use $y+$ equation ;

$$y^+ = \frac{\Delta y}{U}\sqrt{\frac{\tau_w}{\rho}} \tag{28}$$

where Δy is the distance from the first node to the wall. It is important to now about y^+, where it is determine the accuracy of the numerical simulation alongside with grid density (Gebreslassie et al., 2012). Smaller y^+ means more sensitive the grid itself. On the other hand, to achieve the efficiency of simulating we have to find which grid sensitivity and which quantity of meshing the result had already converged. As we can see on the Table 1. Because the results had already converged on fine till finest with slightly different result, we use the grid quantity that give the result before the converging happen.

4.2 Validation

To see how valid the results are, we compare it with other journal experimental results. By using the same properties of the ship and the foil, we compare our numerical results with the experimental results done by Kumagai et al. (2015). To achieve below 10% of error, we used trial and error methods to see which setup has the closest results as possible. By making the same condition as the experimental results done by Kumagai et al. (2015) we got that our setup results having errors below 10%, as described in table 1. From the Table 1. we can see that our average error is 1,93% which is acceptable to continue our numerical setup (Duncan, 1981).

5 RESULTS AND DISCUSSIONS

The result that we got is the force acting on plate c which is the viscous drag that acting along the plate. The focus is on the drag reduction caused by the WAIP that vary on the chord length and angle of attack by compare it with the viscous drag acting along the plate without WAIP installed. The relation between chord length, angle of attack and drag reduction can be depicted on Table 1 which θ, U, D_b, ΔD_b and D_R is angle of attack of the foil, water inlet speed, total drag on plate c, drag reduction and drag reduction percentage on plate c respectively.

On the angle of attack, the less drag reduction that we got caused by the depression (w) which is bigger as the tip of the foil tend to go deeper as the increase of the angle. Besides the creation of the bubble by the flow is getting harder, the mixing flow between air and fluids mostly appeared on the after position of the foil. Moreover, bigger angle of attack make the upcoming flow from $x+$ axis hit the foil wall much bigger. Which make the flow harder to cross and hardly pulling air into the flow.

By using ANSYS post-processing, the creation of bubble can be seen by looking on the pressure area. On the image, the low pressure area mostly occur on the upper surface of the foil and after the foil which is located below the plat c and coated it. By using the volume of fluid model on this setup, the differences between pressure occur among regions caused by the 2 phases flow between air and fluid. Between those figure we can see that the attachment of 20°50mm foil produce more low pressure than the attachment of 12°40mm.

Table 1: Error Percentage of Setup Results

Type	θ	Db (Exp)	Db (Num)	ΔDb	%Error
Bare	Bare	181.485	173.55	-7.935	-4.37
WAIP	12	167.751	168.241	0.49	0.29
WAIP	16	166.77	168.331	1.56	0.94
WAIP	20	164.808	168.281	3.47	2.11
Error					1.93

On 30 mm foil's chord length the increase of the angle of attack decrease the force experienced by the plat. The biggest drag reduction output comes from the biggest angle of attack used, by 3.13% DR. On 40 mm chord length it gives the same trend result, so the biggest drag reduction output alos comes from the biggest angle, with 3.103% DR. This trend also happen on 50 mm foil's chord length, with 3.24% DR.

This phenomena explain the bigger C_p/C_d value the bigger net power saving value done by Kumagai et al. (2015). Where on 6^{th} formula, we can see that the C_p/C_d value relatively bigger as the increase of the chord length and the angle of attack. However, we cannot conclude that bigger angle of attack and longer chord length of the foil surely produce bigger drag reduction on plate E. We can see the lowest drag reduction that is obtained is on the middle of the chord length range. We can also see the fact that on chord length 30mm, the correlation of bigger angle can obtain bigger drag reduction is cannot be said as a globally correct argument. But the same phenomena does not apply to the changing chord length with the same value of angle of attack. On the same degree (angle of attack) variable except 12°the biggest Drag Reduction output still coming from the biggest chord length. But the trend is different, where the second biggest drag reduction output does not come from 40 mm foil's chord length yet it comes from the smallest foil's chord length of 30 mm. On the other hand, the resulted data on 12°variable shows us that the biggest drag reduction occurs on 30 mm, the second biggest drag reduction comes from 50 mm, still the smallest drag reduction is coming from 40 mm chord length.

The chord length of the foil that varied is affecting the Reynold number on the foil which is affect the coefficient pressure. Bigger coefficient pressure that the foil can obtain produce bigger negative pressure on the back of the foil that affecting the entertaining of atmospheric air as can be seen on Figure 1. The effect of Reynold number on coefficient pressure of the foil cannot be 100% predicted especially on big angle of attack. Therefore, the appropriate design can be obtained by using trial and error method.

The changing of drag reduction that occurs on the plate comes from the flow produced by the foil. The characteristic of flow which was occurring on plate will occur differently because of the properties of the foil itself. This properties of the foil occur because of the changing of the chord length. Then the changing of the chord length make the Reynold Number of the flow occurred differently. Which is also makes the different-kind of boundary layer. This unique characteristic of the foil has already been explained in the foil's curve data (Naca Properties).

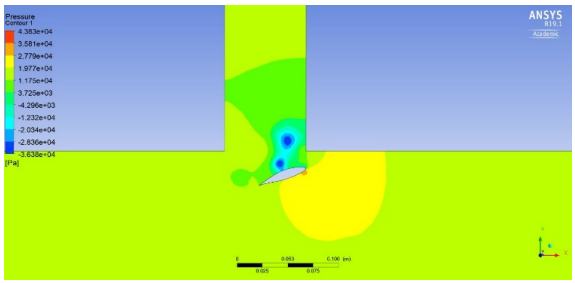

Figure 6: Pressure Area Condition 1

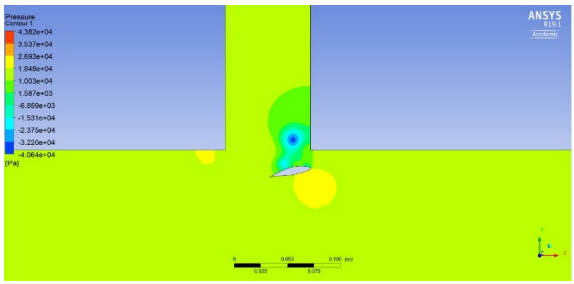

Figure 7: Pressure Area Condition 2

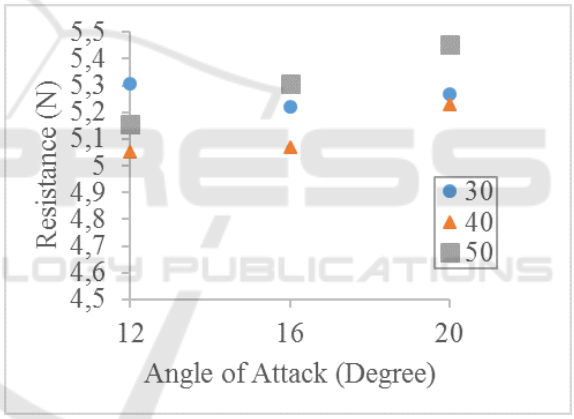

Figure 8: Drag Reduction

Table 2: Numerical Result of Influence of Hydrofoil

θ	U (m/s)	Db (N)	Δ Db	DR (%)
bare	5.6	173.55	-	-
12	5.6	168.2417	-5.3083	3.059
16	5.6	168.3313	-5.2187	3.102
20	5.6	168.2817	-5.2683	3.130
12	5.6	168.4979	-5.0521	3.002
16	5.6	168.479	-5.071	3.010
20	5.6	168.3218	-5.2282	3.103
12	5.6	168.3492	-5.1558	3.063
16	5.6	168.2437	-5.3063	3.151
20	5.6	168.0972	-5.4528	3.241

6 CONCLUSION

From this research we can see that bigger angle will give lesser drag reduction on the plat c while the longer the chord length give bigger drag reduction on

the plat c. On the other hand, smaller drag reduction just make the air entrances the flow a bit harder and longer chord length of the foil just make the resistance appendages slightly bigger. In this research we choose the angle of attack 20°and chord length 50 mm because they were giving the biggest amount of drag reduction among others by 3.241% drag reduction. In the future, we hope that the friction losses which is occur on the foil will be in the future journal.

ACKNOWLEDGEMENTS

Authors are thanks to Department of Mechanical Engineering, Faculty of Engineering, Universitas Indonesia for making facility available and also grant PITTA No. 2561/UN2.R3.1/HKP05.00/2018.

REFERENCES

Cui, Z., Fan, J. M., and Park, A.-H. (2003). Drag coefficients for a settling sphere with microbubble drag reduction effects. *Powder technology.*, 138(2):132.

Duncan, J. H. (1981). An Experimental Investigation of Breaking Waves Produced by a Towed Hydrofoil. *Proceedings of the Royal Society of London. Series A, Mathematical and Physical Sciences*, 377(1770):331–348.

Gebreslassie, M., Tabor, G., and Belmont, M. (2012). Cfd simulations for sensitivity analysis of different parameters to the wake characteristics of tidal turbine. *Open J. Fluid Dyn.*, 2.

Kodama, Y., Kakugawa, A., Takahashi, T., and Kawashima, H. (2000). Experimental study on microbubbles and their applicability to ships for skin friction reduction. *International Journal of Heat and Fluid Flow International Journal of Heat and Fluid Flow*, 21(5):582–588.

Kumagai, I., Kushida, T., Oyabu, K., Tasaka, Y., and Murai, Y. (2011). FLOW BEHAVIOR AROUND A HYDROFOIL CLOSE TO A FREE SURFACE. *Vis Mech Proc Visualization of Mechanical Processes*, 1(4).

Kumagai, I., Nakamura, N., Murai, Y., Tasaka, Y., and Takeda, Y. (2010). A new power-saving device for air bubble generation: hydrofoil air pump for ship drag reduction. In *Proceedings of the International Conference on Ship Drag*.

Kumagai, I., Takahashi, Y., and Murai, Y. (2015). Power-saving device for air bubble generation using a hydrofoil to reduce ship drag: Theory, experiments, and application to ships. *Ocean Engineering*, 95:183 – 194.

Mohanarangam, K., Cheung, S. C. P., Tu, J. Y., and Chen, L. (2009). Numerical simulation of micro-bubble drag reduction using population balance model. *Ocean Engineering*, 36(11):863 – 872.

Muste, M., Yu, K., Fujita, I., and Ettema, R. (2009). Two-phase flow insights into open-channel flows with suspended particles of different densities. *Environmental Fluid Mechanics*, 9:161–186.

Ockfen, A. E. and Matveev, K. I. (2009). Aerodynamic characteristics of NACA 4412 airfoil section with flap in extreme ground effect. *International Journal of Naval Architecture and Ocean Engineering*, 1(1):1 – 12.

Olazabal-Loumé, M., Danvin, F., Julien, M., and Aupoix, B. (2017). Study on k-w shear stress transport model corrections applied to rough wall turbulent hypersonic boundary layers.

Pang, M. J., Wei, J. J., and Yu, B. (2014). Numerical study on modulation of microbubbles on turbulence frictional drag in a horizontal channel. *Ocean Engineering*, 81:58 – 68.

Series A (1779). *Mathematical and Physical Science*. Number 377.

Shereena, S. G., Vengadesan, S. N., Idichandy, V. G., and Bhattacharyya, S. K. (2013). Cfd study of drag reduction in axisymmetric underwater vehicles using air jets.

Uhlman, J. S. (1987). The Surface Singularity Method Applied to Partially Cavitating Hydrofoils. *Journal of Ship Research*, 31(02):107–124.

Yanuar, Gunawan, Sunaryo, and Jamaluddin, A. (2012). Micro-bubble drag reduction on a high speed vessel model. *Journal of Marine Science and Application*, 11(3):301–304.

Zhang, J., Yang, S., and Liu, J. (2018). Numerical investigation of a novel device for bubble generation to reduce ship drag. *International Journal of Naval Architecture and Ocean Engineering*, 10(5):629 – 643.